6th European Conference on Computational Mechanics (ECCM 6)
7th European Conference on Computational Fluid Dynamics (ECFD 7)
11 – 15 June 2018, Glasgow, UK

NUMERICAL INVESTIGATION OF UNLOADING EFFECTS DUE TO EXCAVATION OF GEOMETRICALLY NON-HOMOGENEOUS STRATIFIED ROCK MASSES USING FINITE ELEMENT ANALYSIS

R. SAUFFISSEAU*, A. AHANGAR ASR

School of Computing Science and Engineering (CSE)
University of Salford, Salford, Greater Manchester, M5 4WT
r.sauffisseau@edu.salford.ac.uk; a.ahangarasr@salford.ac.uk

Key Words: Rock masses, unloading, finite element.

Abstract. With growth of population in the cities and lack of suitable land for construction and development in urban areas, buildings are now reaching heights and depths (basements) demanding larger and deeper foundations. Open-cut excavations are amongst the main concerns for projects such as airports in mountainous regions, the Panama Canal, mines, dams, motorways and railways [2]. These excavations inevitably create unloading conditions in the ground in various directions which can lead to creep or sudden failures of vertical faces. In this research, unloading conditions as a result of excavations are observed for rock masses. A realistic stratified rock mass configuration including layers with various mechanical properties such as disturbance factor (D), uniaxial compressive strength (UCS), geological strength index (GSI), Poisson's ratio (nu') and the intact rock parameter (m_i) is modelled. The Finite Element package PLAXIS 2D is used to assess the response of the rock mass to the excavation, looking at displacements (overall and localised) to understand and predict possible failures in rock masses with the ultimate aim of making the excavation process in rocks safer and more economically feasible for the industry. Two cases are presented using the same rock mass arrangement without and with a crack induced on one side of the excavation to target the impact of the crack and weaker rock layers on the overall stability.

1 INTRODUCTION

Buildings tend to be high-rise in the cities with quite large basements (used as carparks etc.). Therefore, deep vertical excavations are required to be created at construction stage to allow for safe battered slopes [10]. There are also demands for larger motorways which means larger cuts must be done through hills and mountains [5] leading to open-cut excavations which are also a main concern in projects like Airports, Building sites, Canals, Dams, Motorways/Rails and Quarries/Pits [2].

The most common techniques for rock excavations are to break down the rock mass into fragments, then it is heaved and made loose to enable excavators and wheel loaders to transport off-site [5]. Techniques used include blasting, drilling, tunnel boring machine (TBM) [11]. Various techniques may be more reliable and efficient in different conditions. A TBM is more efficient with very hard rock [9], blasting is mostly used when a TBM cannot be acquired or if

the shape/size of the tunnel is not doable by TBM (circular only). Blasting is also used when very large volumes of rock need to be disintegrated (quarries) [18].

With time, rock masses accumulate energy through self-compaction and the increasing loads at the surface with the deposition of sediments or man-made structures resting on the earth's surface. Undertaking vertical excavations in these rock masses can lead to the release of the energy which is known as strain energy [15]. Then, displacements through dilation will occur in which foliated rocks would display a higher dilation compared to crystalline rocks [12].

According to Jaeger [7], one of the main aspects of rocks which affect the stability of a rock mass is the level at which they are disturbed i.e. existence of many interfaces within the body of rock masses. To measure how disturbed a rock mass or strata is, the valuable variable of the Hoek-Brown criterion which is the disturbance factor, D, is used.

Rock can fail mainly in two possible ways. The first is by having a sample reaching its ultimate strength leading to crushing (crystalline bond broken) and the other, which a lot more common, is due to the failure (more commonly sliding) in the interfaces between intact rock blocks creating the rock mass [19].

Natural rock slopes are stratified, and the consequence of stratification is the presence of many interfaces. Depending on the arrangement of these layers, the three-dimensional geometry of the interface will vary and induce distinct failure forms [3, 14]: Plane failure, Wedge failure, Circular failure, Block toppling, Flexural toppling and Rockfalls.

Hoek Brown (HB) is a non-linear criterion to analyse stress conditions and subsequently the stability conditions in rocks and is formulated as [4]:

$$\sigma'_1 = \sigma'_3 + C_0(m_b \frac{\sigma'_3}{C_0} + s)^a \quad (1)$$

Where: σ'_1 is the major principal stress; σ'_3 the minor principal stress; $C_0 (= UCS = sigma\ ci)$ the uniaxial compressive strength; m_b the Hoek-Brown material constant for rock masses (a measure of integrity of the rock); s and a material constants respectively showing blockiness and surface condition of the rock [4]. Some parameters in this equation also depend on other parameters such as:

$$m_b = m_i exp\left(\frac{GSI - 100}{28 - 14D}\right) \quad (2)$$

m_b is a reduced value for m_i (the Hoek-Brown material constant for intact rock, obtained from regression analysis based on triaxial tests [17] for broken rock which is modified by the GSI (Geological Strength Index) and D, the Disturbance factor. Equations 3 and 4 also show the relationship between the GSI and D with other material constants *s* and *a* (*e=exp=exponential*):

$$s = exp\left(\frac{GSI - 100}{9 - 3D}\right) \quad (3)$$

$$a = \frac{1}{2} + \frac{1}{6}\left(e^{-\frac{GSI}{15}} + e^{-\frac{20}{3}}\right) \quad (4)$$

In this research, the Finite Element [13] software PLAXIS 2D is used. PLAXIS 2D is based on continuum mechanics and uses the deformation theory to analyse the soils/rocks models [1, 8]. Input data for each rock material includes mechanical material properties i.e. unit weight, the stiffness parameters (Young's modulus of elasticity (GPa) and Poisson's ratio) as well as constitutive model (Hoek-Brown) parameters (uniaxial compressive strength (MPa), Hoek-

Brown intact material constant (m_i), geological strength index (GSI), and disturbance factor (D)- [16]).

Each element used in the mesh is composed of a set number of nodes and stress points. PLAXIS 2D has two options for the mesh, 6-noded or 15-noded elements. According to Vermeer [16], 15-noded elements are made of 12 stress points which increases the accuracy of the results as opposed to the 6-noded elements with only 3 stress points (6 nodes). In the research presented, deformations are expected to be very small since the material is rock (stiff and almost rigid) and therefore, 15-noded elements are used for improved accuracy.

2 MODEL DEVELOPMENT

Based on a case study from the literature [6], the PLAXIS 2D model was created using the latest version of the software (v. 2016.1). A layered rock mass was simulated with all layers laid mainly horizontally. Orientations and depths of the rock layers as well as variations in inclinations in interface levels were obtained from the case study to ensure a closest possible simulation to the reality.

It was assumed that for all excavation stages, the excavation technique will be non-disruptive and will not cause any damages to the rock mass (no impact, vibrations, etc.) which could induce failures or any other movements in the rock mass.

Based on the geometry of the case study, a series of rock types were used to create a common rock mass used in the following two model cases created:

1) Case 1: Rock mass model without cracks near the vertical face

In this case, the rock mass presented in Figure 1 was modelled to inspect the behaviour of the slope face when unloading (removing lateral support provided by the rock being excavated to the rock face in the excavation) through excavation.

Using PLAXIS 2D, a ‘very fine’ mesh (0.03 fineness factor) was generated which led to a model with 4,820 elements and 39,976 nodes.

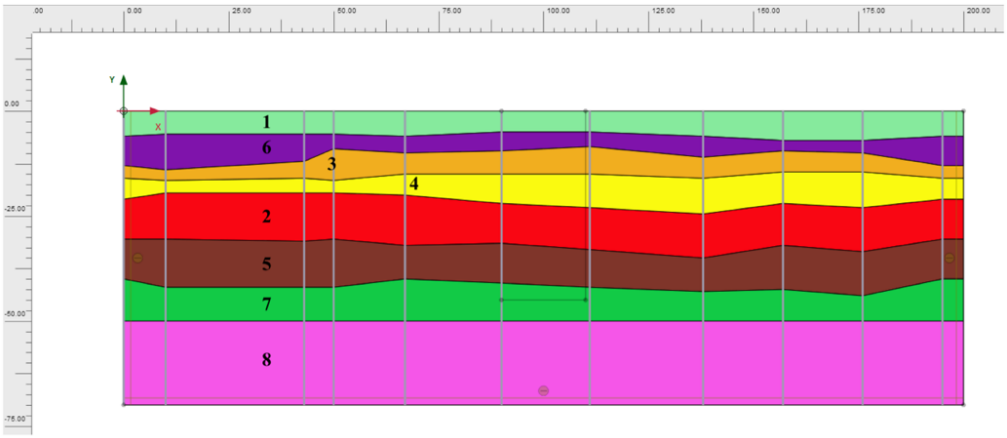

Figure 1: Case 1 model on PLAXIS 2D - layers numbering linked to Table 2 to present rock material properties

2) Case 2: Rock mass with cracks available near excavated face

A crack was simulated on the left side of the excavation slope to observe the change in behaviour of the rock mass when excavating and to observe the crack presence effect on deformations, displacements and stress conditions (Figure 2).

Similar to Case 1, a 'very fine' mesh (0.03 fineness factor) was generated which led to a greater number of elements and nodes in the model: 5,293 elements and 43,818 nodes. A local mesh refinement was created around the crack zone to locally increase the accuracy of the analysis.

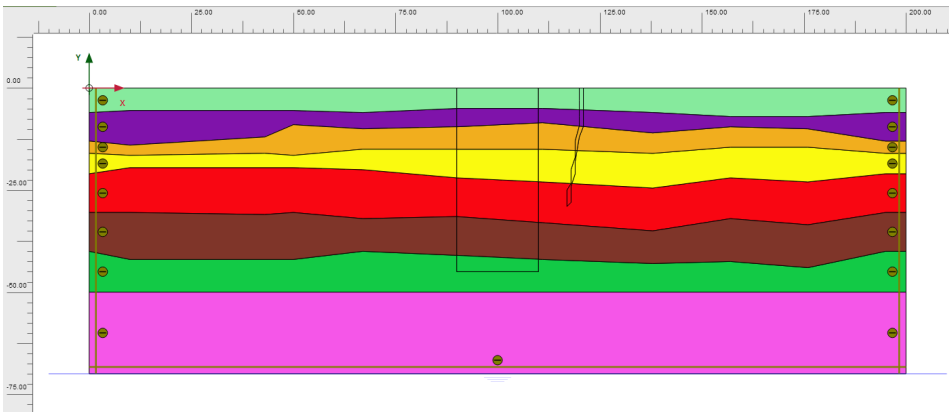

Figure 2: Case 2 model on PLAXIS 2D – crack presence is simulated

In both cases, points were selected to obtain accurate displacement data at different depths on both sides of the excavation. Points A and F (Table 1) are located at the top of the excavation edge, B and C at mid-height on the excavation faces of the Sandstone layer respectively on both sides of the excavation (Table 1 and Figure 1), D and E at mid-height on the excavation faces of the Diabase layer respectively on both sides of the excavation (Table 1 and Figure 1) and G is only applicable to Case 2 and is located at the top of the crack (left edge) – Figure 3. In case 2, the horizontal at points A and G is expected to be similar due to their proximity and that they are located on the rock mass' surface. All points coordinates are presented in Figure 3 and Table 1.

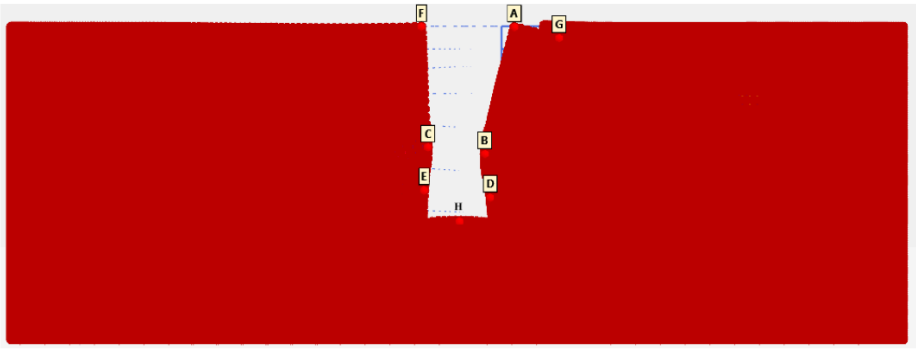

Figure 3: Location of the points on the model, see Table 1 for coordinates

Table 1: Point coordinates for displacement results - Points A-F and H have the same coordinates in both cases and point G only exists in Case 2 (Figure 3)

Point	x (m)	y (m)
A	110	0.00
B	110	-27.94
C	90	-26.77
D	110	-37.48
E	90	-36.16
F	90	0.00
G (Case 2 only, crack)	120	0.00
H (Middle of bottom of the excavation)	100.9	-45.00

Table 2: Rock mass material properties for the Hoek-Brown criterion used in PLAXIS 2D*

Materials	ID	Material Model	Drainage type	Colour	Unit Weight	E' (Gpa)	nu'	sigma ci (Mpa)	mi	GSI	D	Type
Limestone	1	Hoek-Brown	Drained		27	40	0.15	62	8.4	60	0.6	Sedimetary
Sandstone	2				20	28	0.1	240	18.8	65	0.6	Sedimetary
Marble	3				27	60	0.3	70	9.3	93	0	Metamorphic
Gneiss	4				27	80	0.12	140	30	90	0	Metamorphic
Diabase	5				29	78	0.18	250	15.2	85	0.15	Igneous
Granite	6				29	55	0.18	120	32.7	91	0.15	Igneous
Basalt	7				29	30	0.17	50	17	89	0.15	Igneous
Quartzite	8				27	100	0.23	310	23.7	99	0	Metamorphic

* ID corresponds to the numbering on the layers on Figure 1. Unit Weight is in kN/m^3, E is the Young's Modulus of Elasticity (GPa), "nu" is the Poisson's ratio, "sigma c" the Uniaxial Compressive Strength (MPa), "mi" the intact Hoek-Brown material constant, GSI the Geological Strength Index and D the disturbance factor.

The Quartzite layer positioned at the bottom of the rock mass modelled is there to provide a sufficient rock thickness as a rigid boundary condition. Additionally, the model rock mass is 200 meters long with a 20m wide excavation created in the middle. Large dimensions are used to provide a sufficiently large model to ensure boundary condition effects do not occur near the zone of study.

In this research water presence is not considered in the analysis, so the water table was placed at the depth of 70.0m in both case models (Figure 1 and Figure 2).

The loading type used in PLAXIS 2D in this research was 'staged construction' which enables the user to observe the behaviour of the rock mass faces at different stages of the excavation and is the closest possible case to how the excavations are created in reality. A 9-phase system was created including PLAXIS standard 'Initial Phase' as well as phases 1 to 8. 'Initial Phase' and 'Phase 1' calculate the initial stress conditions before any excavation takes place. In 'Phase 2' followed by other phases till 'Phase 8', a layer of rock is taken out as part of the excavation process (i.e. in Phase 2 taking layer 1 out,…in Phase 5 taking layer 6 out…to Phase 8 where taking part of layer 7 out - Figure 1).

The model assumes rigid rock bodies and 'Rigid' interfaces are defined. The excavation is 20 metres wide (both cases) and the crack, located 10 metres to the right of the right edge (Figure 2), has a varying width starting from 1m at the top and narrowing down in depth (Case 2 only).

3 ANALYSIS AND RESULTS

3.1 Case 1

After the analysis being completed in Case 1 using the Finite Element PLAXIS 2D model (as detailed above), the following deformed mesh was obtained (Figure 4):

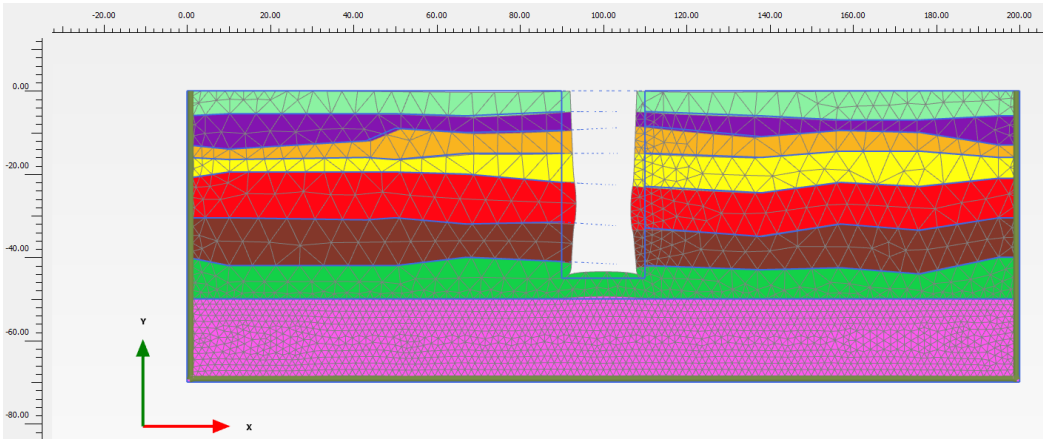

Figure 4: Case 1, deformed mesh (deformations visible on the output are not to scale)

It can be observed that the Sandstone layer (4) bulges out more compared to other layers meaning the horizontal displacement at the half-depth of the Sandstone layer is greater than of the other layers. To check that this behaviour is a result of the non-homogeneity and stratification of the rock mass, the same excavation was analysed on a homogeneous Sandstone rock mass. Analysis results presenting displacements pattern are shown in Figure 5.

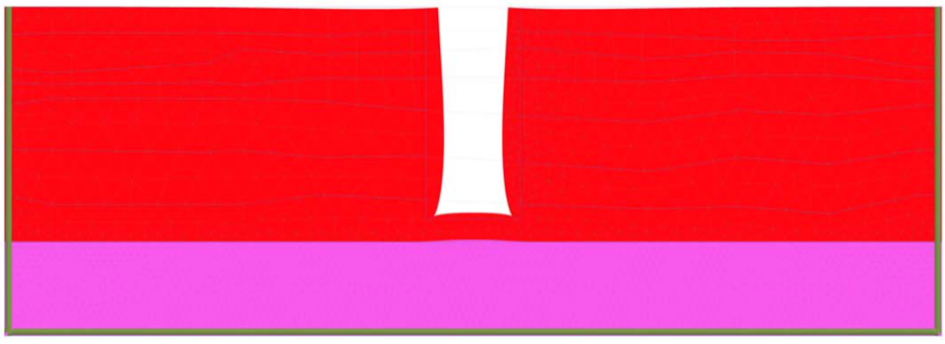

Figure 5: Sandstone only - deformed mesh showing displacements in the rock face after excavation

In Figure 4, from the top of the rock face to the top of the sandstone layer, the rock face linearly and progressively moves outwards and suddenly bulges out as the face reaches the sandstone. A greater bulge occurs in the sandstone layer but then the trend goes back to what it was above the sandstone layer as the excavation continues afterwards until reaching the bottom of the excavation. However, in Figure 5, Sandstone rock mass (except for the Quartzite base), a smooth curved mesh deformation is observed without any localised bulging. In the layered

analysis case the horizontal displacements of the rock mass on both sides of the excavation are similar and maximum displacement regions are located in the Sandstone layer (Figure 6).

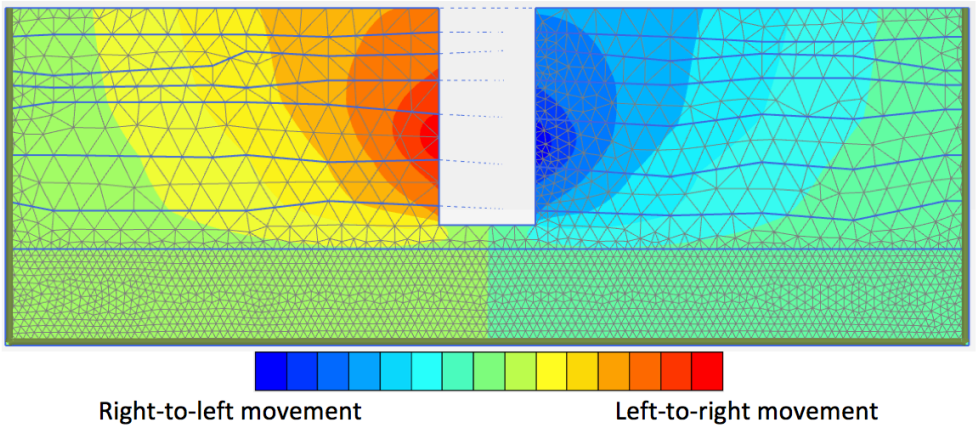

Figure 6: Horizontal displacements - Case 1

3.2 Case 2

In Case 2 the analysis was repeated considering presence of a crack. The deformed mesh after completion of the analysis is shown in Figure 7.

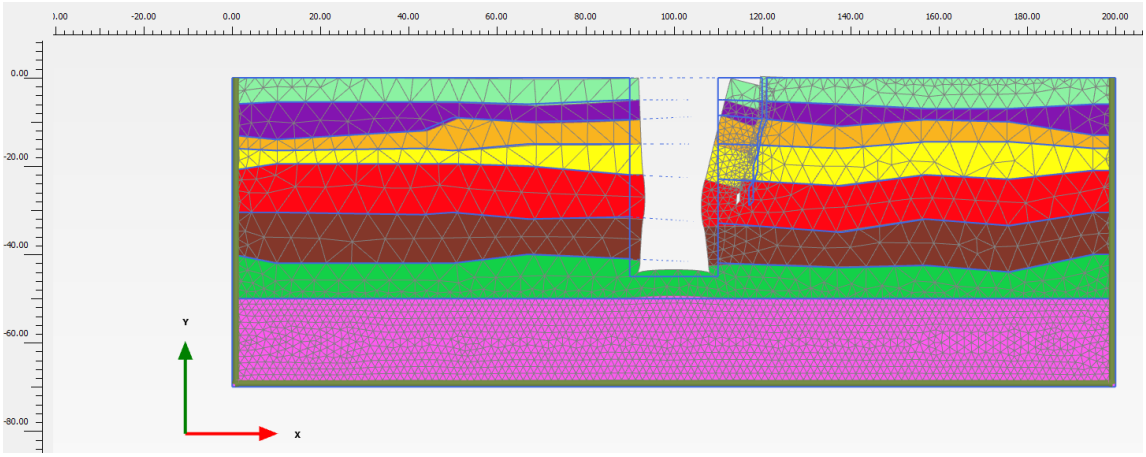

Figure 7: Case 2, deformed mesh (deformations visible on the output are not to scale)

On the left excavated rock face in Case 2 (Figure 7), the behaviour is similar to Case 1 (Figure 4) with a linear deformation with depth and the Sandstone layer bulging outwards. However, on the right side, the crack creates major differences in the behaviour of the rock face. It can be observed that the top part of the block (rock mass section between crack and excavation wall) moves toward right closing the crack. At the level of the Sandstone, a right-to-left movement is observed with some bulging as opposed to the left-to-right movement of the top of the rock excavation face. Figure 8 shows the horizontal displacement contour plot for Case 2 after analysis being completed.

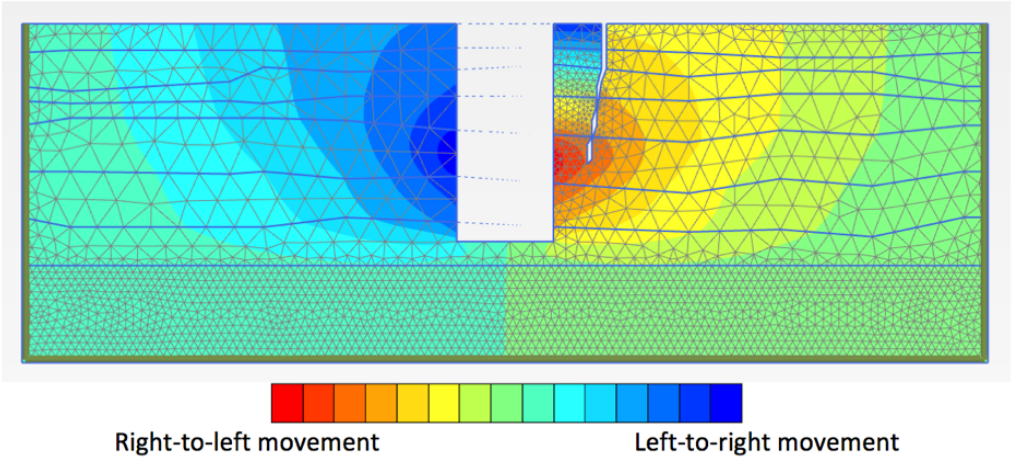

Figure 8: Horizontal displacement - Case 2.

3.3 Common observations in both cases

As expected the behaviour of the rock excavation face in the left side during excavation is similar in both cases. Also heaving happens at the base of the excavation in both cases due to unloading induced by the excavation at every stage (Figure 4 and Figure 7 – after final stages of excavation in both cases). Maximum heaving was observed in phase 5 when the Gneiss (layer 4 in Figure 1 and Figure 2) was removed allowing the Sandstone to dilate and expand in the only possible direction - upwards (movement restrained in any other direction). The heaving in both cases after completion of the final stages of analyses were similar magnitudes (measurements were taken at point H – Table 1). Figure 8 shows a schematic representation of the deformations occur in the excavation faces with (left face) and without (right face) crack presence.

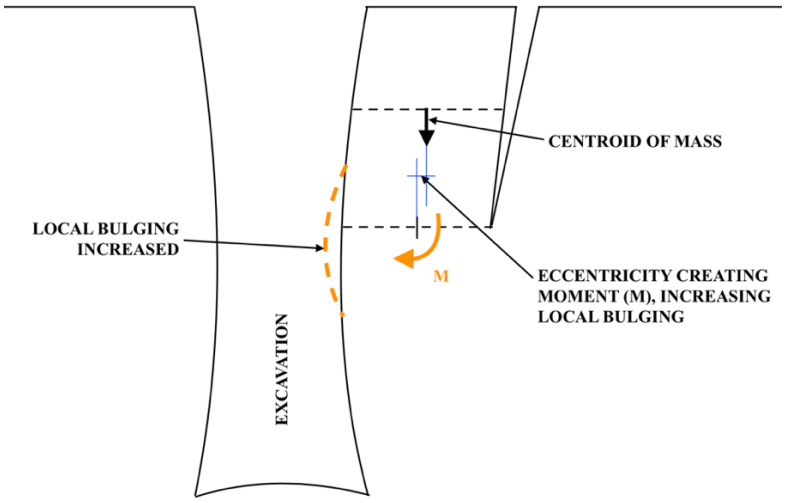

Figure 9: Schematic representation of excavation face deformations with and without crack presence

4 DISCUSSIONS AND CONCLUSIONS

Effect of unloading due to excavation in rock masses on the deformations occurring on the faces of an excavation with and without presence of a crack has been investigated in the study using finite element model analysis. Larger lateral deformations occur at greater depth generally as the excavation progresses and these deformations are particularly larger where the materials are weaker under large stresses.

As a general observation and based on the horizontal displacement values obtained in Case 1 and Case 2 at several points, the crack has a significant impact on the behaviour of the rock face on which it is positioned. In Case 1, point A indicates a right-to left movement ($3.9 \times 10^{-7} m$) whereas in Case 2, the overall movement is left-to-right (horizontal displacement of $18 \times 10^{-7} m$ at point A).

At points C and E (Table 1), no significant differences were observed between both cases (same ground conditions and geometry were considered) however, at point B (Table 1), the right-to-left deformation is greater in Case 2 compared to Case 1 which can be explained by the impact that the crack has on the behaviour of the excavated rock face. When deformations occur i.e. – top of the rock mass moving from left-to-right (Figure 7 and Figure 8), the centre of mass is shifted to the right creating an eccentricity as shown in Figure 9 which produces a moment favourable to additional local bulging.

In Case 2, the left-to-right movement of the rock body induced by the crack is affected by the inclination of the crack which starts 10 metres away from the excavation edge at the top but gets closer to the excavation (as close as 6.5m to the rock excavation face at the depth of 27.5m). Due to the crack's inclination, the centroid of mass of the rock between the excavation and the crack is shifted to the right which leads to the closure of the crack. This can be easily observed from the horizontal displacement of points A and G (Figure 3 and Figure 7). It can be concluded increases inclination will strengthen this effect.

In both model Cases 1 and 2, the maximum amount of bulging observed was in the Sandstone rock layer which seems to be the least strong rock layer according to Table 2. Since sandstone layer is also subjected to a high level of vertical stresses (weight from all rock layers above - Figure 1 and Figure 2) relative lateral deformation occurring in the layer are greater.

Heaving at the bottom of the excavation also occurred at every stage in both model cases of excavation with the maximum value relating to the sandstone layer when the layer on top of it (layer 4, Gneiss, in Figure 1 and Figure 2) was removed. In the rock mass arrangement used in this study, heaving at point H in both cases (Figure 3, Figure 4 and Figure 7) was of similar magnitude signifying the fact that crack condition (location, size and shape) does not have a significant impact of the heaving of the excavation base. In other cases, this may become untrue and cracks closer to the bottom of the excavation will impact on the behaviour.

REFERENCES

[1] Brinkgreve, R., Kumarswamy, S., Swolfs, W., Waterman, D., Chesaru, A., Bonnier, P., & Haxaire, A. (2011). Plaxis 2D Scientific Manual. *I R*.

[2] Church, H. K., & Robinson, J. (1988). *Excavation planning reference guide*: McGraw-Hill.

[3] Craig, R. F. (2004). Craig's soil mechanics. In (7th ed. ed.). London.

[4] Eberhardt, E. (2012). The hoek–brown failure criterion. In *The ISRM Suggested Methods for Rock Characterization, Testing and Monitoring: 2007-2014* (pp. 233-240): Springer.

[5] Harber, A., Nettleton, I., Matheson, G., McMillan, P., & Butler, A. (2011). *Rock engineering guides to good practice: road rock slope excavation*.
[6] He, M., Li, X., Liu, B., & Xu, N. (2007). Three-dimensional modeling of borehole data cored from engineering rock mass. *Selected Publications from Chinese Universities, 1*(3), 334-339. doi:10.1007/s11709-007-0044-9
[7] Jaeger, J. (1971). Friction of rocks and stability of rock slopes. *Geotechnique, 21*(2), 97-134.
[8] Koppel, A., & Oja, J. (2010). *Continuum mechanics*. New York: New York : Nova Science Publishers.
[9] Maidl, B., Schmid, L., Ritz, W., & Herrenknecht, M. (2008). *Hardrock tunnel boring machines*: John Wiley & Sons.
[10] Ng, C. W., Simons, N. E., & Menzies, B. K. (2004). *A short course in soil-structure engineering of deep foundations, excavations and tunnels* (Vol. 5): Thomas Telford.
[11] Palmström, A. a. (2015). *Rock engineering* (Second edition. ed.): London : ICE Publishing.
[12] Pérez-Rey, I., Alejano, L. R., Alonso, E., Arzúa, J., & Araújo, M. (2017). An Assessment of the Post-peak Strain Behavior of Laboratory Intact Rock Specimens Based on Different Dilation Models. *Procedia Engineering, 191*, 394-401. doi:10.1016/j.proeng.2017.05.196
[13] Rao, S. S. (2005). The finite element method in engineering. In (4th ed. ed.). Amsterdam ; Boston, MA: Amsterdam ; Boston, MA : Elsevier/Butterworth Heinemann.
[14] Simons, N. E. (2001). A short course in soil and rock slope engineering. In B. K. Menzies & M. C. Matthews (Eds.). London: London : Thomas Telford.
[15] Tao, M., Li, X., & Li, D. (2013). Rock failure induced by dynamic unloading under 3D stress state. *Theoretical and Applied Fracture Mechanics, 65*, 47-54. doi:10.1016/j.tafmec.2013.05.007
[16] Vermeer, P. (1993). PLAXIS 2D reference manual version 5. *Balkema, Rotterdam/Brookfield, 70*.
[17] Yang, X. L. (2017). Effect of pore-water pressure on 3D stability of rock slope. *International Journal of Geomechanics, 17*(9), <xocs:firstpage xmlns:xocs=""/>. doi:10.1061/(ASCE)GM.1943-5622.0000969
[18] Zhang, Z.-X. a. (2016). *Rock fracture and blasting : theory and applications*: Amsterdam, Netherlands : Butterworth-Heinemann.
[19] Zou, D. a. (2017). *Theory and Technology of Rock Excavation for Civil Engineering*: Singapore : Springer Singapore : Imprint: Springer.